3

A Conceptual Model for the Nonlinear Dynamics of Edge-localized Modes in Tokamak Plasmas

Todd E. Evans[1], Andreas Wingen[2],
Jon G. Watkins[3] and Karl Heinz Spatschek[2]
[1]*General Atomics,*
[2]*Institute for Theoretical Physics, Heinrich-Heine-University,*
[3]*Sandia National Laboratory,*
[1,3]*United States*
[2]*Germany*

1. Introduction

High performance magnetically confined toroidal plasmas, such as those required for the operation of a tokamak based fusion power plant, suffer from a troubling type of repetitive edge instability known as edge-localized modes (ELMs). Magnetohydrodynamic (MHD), peeling-ballooning, theory predicts that these instabilities are driven by a large current density and pressure gradient that forms at the plasma edge as a consequence of the enhanced confinement levels achieved in high performance H-mode plasmas. Although ELMs are a common feature of high confinement tokamak plasmas, there are significant gaps in our understanding of how these instabilities scale with the geometry of the plasma and operating conditions expected in large tokamaks that are required for the generation of fusion power. Thus, there is an urgent need for a model that can be validated with experimental data from existing smaller tokamaks.

Here, we present a conceptual model describing the topological evolution of the magnetic separatrix, in a tokamak plasma with a dominate lower hyperbolic point. Subsequently, the nonlinear dynamics of the ELM instability, prescribed by the evolving separatrix topology, is discussed. The model invokes a feedback amplification mechanism that causes the stable and unstable invariant manifolds of the separatrix, comprising a "homoclinic tangle" (Guckenheimer & Holmes, 1983), to grow explosively as the topology of the separatrix manifolds unfold. The amplification process is driven by the rapid growth of helical, field-aligned, thermoelectric currents that flow through relatively short edge plasma flux tubes connecting high heat flux wall structures, known as divertor target plates, on both sides of the plasma. These thermoelectric currents produce magnetic fields that couple to the separatrix and modify its 3D (topological) structure. As the lobes of the separatrix tangle grow, their area of intersection with the divertor target plates increases along with the size of the flux tubes connecting target plates on both sides of the plasma. This increases the thermoelectric current flow and completes the feedback loop. Numerical simulations have shown that our model is consistent with measurements of the currents flowing between the target plates and with camera images of the heat flux patterns on the divertor target plates

Source: Nonlinear Dynamics, Book edited by: Todd Evans,
ISBN 978-953-7619-61-9, pp. 366, January 2010, INTECH, Croatia, downloaded from SCIYO.COM

(Wingen, et al. 2009a). In addition, this model suggests that nonaxisymmetric external magnetic coils can be used to force higher order separatrix bifurcations to prevent ELMs.
In the following sections, we discuss why ELMs are an important problem in tokamaks, review what is known experimentally and theoretically about the characteristics of ELMs, present a conceptual framework for the nonlinear evolution of an ELM and discuss results from numerical simulations of the proposed model. We show a sequence of topological bifurcations that are observed in the numerical simulations and discuss how these result in a separatrix topology that produces heat flux patterns which are consistent with those measured by infrared cameras in the DIII-D (Luxon, 2002) tokamak. A general description of tokamaks and tokamak physics is given by Callen et al., (1992), Evans (2008) and Wesson (2004).

2. Properties of ELMs in high performance tokamak plasmas

2.1 ELM dynamics

Type-I ELMs are naturally occurring MHD instabilities that release large bursts of particles and energy from the boundary of the plasma (Suttrop 2000). These very fast growing instabilities share properties that are somewhat similar to the eruption of prominences and flares from the solar photosphere (Evans, et al., 1996). More specifically, expanding hot plasma filaments carrying energy, particles and momentum away from the confined plasma volume into the surrounding space are associated with these complex dynamical plasma events that form on the surface of the sun and at the edge of a tokamak discharge. Tokamaks operating in high confinement H-modes, with strong edge transport barriers, rely exclusively on the formation of a large pressure gradient near the surface of the plasma to obtain sufficiently high central temperatures and densities to carry out fusion energy experiments in these devices. These large pressure gradients are believed to drive edge MHD instabilities, referred to as peeling-ballooning modes, that are responsible for the onset of ELMs (Snyder, et al., 2005). Since ELMs periodically release particles and energy from the edge of the plasma, they limit the size of the pressure gradient that can be obtained in tokamaks (Fenstermacher, et al. 2003). Scaling studies suggest that this limits the maximum temperature of the core plasma and thus the ultimate performance of the tokamak (Loarte, et al. 2003). In addition, the impulsive energy and particle flux released by ELMs can cause a significant enhancement in the erosion of solid surfaces that make up the internal walls and divertor components of the tokamak. The impulsive loading of these structures due to ELMs releases non-hydrogenic impurities as a result of enhanced solid surface erosion. These impurities change the properties of the divertor plasma and can be transported out of the divertor chamber into the region of the scrape-off layer (SOL) plasma located between the separatrix in the main chamber walls of the tokamak. While ELMs tend to prevent the eroded divertor impurities from penetrating deeply into the high temperature region of the core plasma, located inside the steep pressure gradient region referred to as pedestal plasma, these impurities can accumulate in steady-state discharges and affect the plasma performance unless the tokamak pumping system is capable of removing this additional particle flux.
ELMs are typically classified by the amount of energy they eject from the pedestal plasma and their dynamical properties. The largest of these instabilities, referred to as type-I ELMs, are capable of reducing the energy stored in the pedestal plasma by as much as 20-25% in tokamaks operating at the highest performance levels (Loarte, et al. 2003). In the largest

tokamaks operating at the present time, this amounts to the ejection of up to 1 MJ of energy within a period of about 200-300 μs. In the next generation of tokamaks that are under construction or being planned, the energy ejected by a single ELM is expected to increase by about a factor of 20. These type-I ELMs are also characterized by an increase in frequency f_{ELM} as the injected power level of the neutral beam heating system P_{NBI} increases and they do not tend to have any clearly identifiable coherent magnetic fluctuations prior to their onset (*i.e.*, magnetic precursors) although an increase in the level of broadband plasma turbulence is sometimes observed prior to their onset. Profiles of the edge electron density (n_e) and temperature (T_e) just before an ELM are shown for a typical DIII-D type-I ELMing discharge in Fig. 1(a) while Fig. 1(b) shows how the n_e profile changes immediately following a type-I ELM.

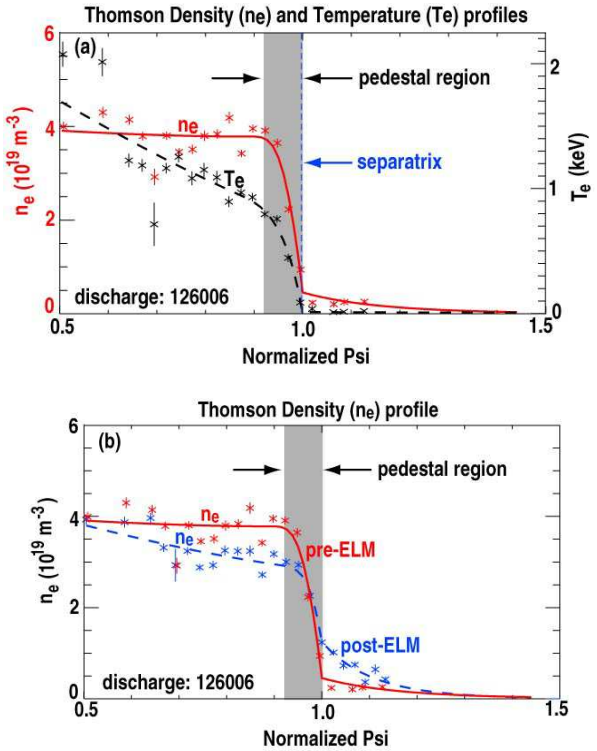

Fig. 1. (a) An example of the steep n_e and T_e profiles, as a function of the normalized poloidal magnetic flux Psi (ψ_N), across the outer region of the plasma inside the separatrix and outside the separatrix in a region referred to as the SOL and (b) the n_e profile before and after an ELM in DIII-D discharge 126006.

As seen in Fig. 1(b), plasma density from the top of the pedestal region inward to approximately 1/2 the radius of the core plasma, at a normalized poloidal magnetic flux Psi (ψ_N) equal 0.5, is ejected into the region outside the separatrix, referred to as the SOL, during the explosive growth period of the ELM instability in a typical high performance, low collisionality, DIII-D type-I ELMing discharge. Type-I ELMs typically have frequencies f_{ELM}

= 10-200 Hz and are triggered when the pedestal pressure gradient ($\alpha_{ped} \propto \nabla p_{ped}$) approaches the critical ideal MHD ballooning limit $\alpha_{ped} \sim 2–3\ \alpha_{crit\_ball}$ (Osborne et al., 2000). They are often characterized by an isolated, very rapid, increase in the deuterium recycling emissions when the particles ejected from inside the separatrix arrive at the divertor target plates or the walls of the tokamak as shown in Fig. 2.

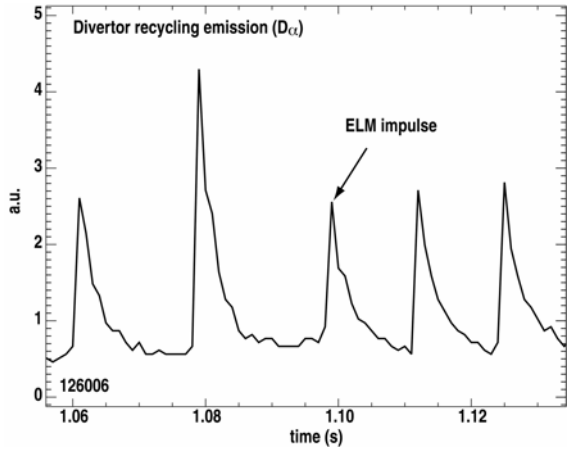

Fig. 2. A series of type-I ELM impulses seen in the lower (primary) divertor deuterium (D_α) recycling emissions during DIII-D discharge 126006 where f_{ELM} = 50→75 Hz is correlated to an increase in the stored energy of the plasma.

A significant fraction of the energy released from the pedestal during type-I ELMs strikes the divertor target plates [see Fig. 5(b) for a view of the DIII-D lower divertor and divertor target plates] along with the particle flux responsible for the spikes in the recycling emissions (Fig. 2). It is this combined, highly impulsive, heat and particle flux that can cause enhanced erosion of the divertor targets and walls in large, high performance, tokamaks leading to a substantial increase of non-hydrogenic impurities released into the divertor and SOL plasmas.

Also associated with these impulsive heat and particle fluxes are large, rapidly growing, electric currents that are an intrinsic part of type-I ELM dynamics. These currents are, in fact, a basic element of the nonlinear model described below. In DIII-D Langmuir probes are used to measure the parallel ion saturation current flowing through the divertor target plates at several radial positions. These measurements show that these currents grow explosively to a saturated amplitude exceeding 1 A/mm² in 50 μs or less during the nonlinear growth of a type-I ELM. Measurements of the toroidal distribution and dynamics of these currents with a toroidal tile current array in DIII-D has shown that they are strongly non-axisymmetric with dominate toroidal mode numbers consisting primarily of n=1 and 2 components (Evans et al., 1995) while the presence of higher n modes has been observed during ELM precursors in some DIII-D discharges (Osborne et al., 2000). As an example of the dynamics involved in the evolution of this current, the data shown in Fig. 3 demonstrates the explosive growth of the instability followed by a slow decay during a single ELM. This data is obtained with two lower divertor Langmuir probes located just outside the 15 mm SOL flux surface with major radii R = 1.500 m and 1.528 m in a double

null (upper and lower hyperbolic point) DIII-D discharge biased upward by 11 mm. The radial structure of this current indicates that the ELM produces a strong interaction with the top of a pump duct more than 120 mm away from the point of intersection of the separatrix with the lower divertor target (Fig. 5 shows a layout of the lower divertor geometry). This data also suggests that current flowing in a type-I ELM may be associated with a relatively ridged structure that forms during its initial explosive growth phase. Finally, it suggests that as the current in this structure decays it appears to rotate past the two Langmuir probes with a rather regular period of $\Delta t \sim 480$ μs (*i.e.*, a toroidal rotation velocity $v_{ELM} = 2\pi R/\Delta t \sim 19.6$ km/s where R is the radial position of one of the Langmuir probes) as indicated by a series of fairly regularly spaced peaks shown in Fig. 3. Signatures such as these have also been seen in the DIII-D midplane reciprocating Langmuir probe data where $v_{ELM} = 13.5$ km/s was observed in plasmas with edge toroidal carbon rotation velocities $v_{carbon} = 22$ km/s (Boedo et al., 2005; Yu et al., 2008).

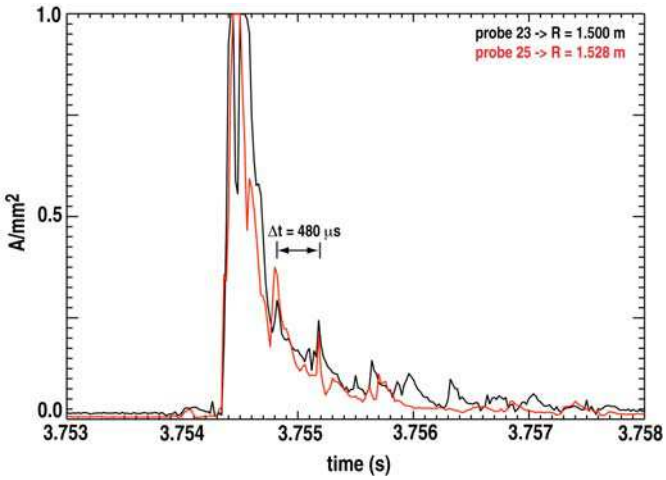

Fig. 3. Time evolution of the plasma current measured by a pair of lower divertor Langmuir probes located 28 mm apart in major radius (R) during an ELM DIII-D discharge 138229.

Type-II ELMs are sometimes observed as the axisymmetric plasma shape becomes more triangular and elongated. They often appear as small, irregular, fluctuations in the D_α data interspersed between the large type-I ELM D_α spikes. Type-II ELMs do not appear to have a distinct P_{NBI} dependence or any signatures associated with coherent MHD precursors and do not seem to be associated with a specific α_{crit} limit (Zohm, 1996). Type-III ELMs are small, relatively high f_{ELM}, instabilities that tend to have lower frequencies as P_{NBI} increases (Osborne et al., 2000). They typically have coherent magnetic precursor modes with frequencies in the 50 kHz range and have low to intermediate toroidal mode numbers (n=5-10). They are often found in relatively high-density, lower P_{NBI}, plasmas with α_{ped} ranging from about 30% to 50% of α_{crit} (Suttrop, 2000). Other types of small ELMs (e.g., type-V) have been identified in spherical tokamaks where they appear only in lower single null plasmas and are often interspersed between large type-I ELMs (Maingi et al., 2005).

The conceptual model proposed here deals exclusively with the nonlinear dynamics and associated topological evolution of the explosive growth seen during the initial growth of

type-I ELMs. The dynamics of the different types of ELMs outlined above, as well as those observed during intermittent transport bursts in low confinement modes (L-modes) are, at the most fundamental level, required to conform to the general framework of this model *i.e.*, the fact that a divergence free vector field, such as the equilibrium magnetic field in a tokamak or stellarator, must ultimately be consistent with a (conservative) Hamiltonian representation such as that prescribed by dynamical systems theory (Guckenheimer & Holmes, 1983; Lichtenberg & Lieberman, 1992).

2.2 ELM topology

Before elaborating the details of the nonlinear type-I ELM model below, it is instructive to briefly describe the global topology of these instabilities. Fortunately, spherical tokamaks such as MAST (Kirk et al., 2004; Kirk et al., 2007) and NSTX (Maingi et al., 2005) are equipped with visible light fast framing cameras that can capture images of type-I ELMs. Figure 4 provides a full view of the plasmas captured during a type-I ELM in MAST.

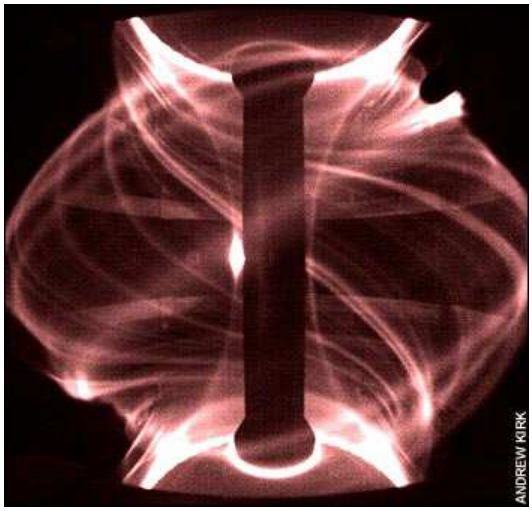

Fig. 4. A wide-angle view of the MAST plasma at one instant in time during the evolution of a type-I ELM (Courtesy of A. Kirk, Culham Laboratory, UK).

Here, the bright emission bands, referred to as ELM filaments, wrap around the outer surface of the plasma in helical patterns that connect the upper and lower divertors. The pitch of these filaments is aligned with the local magnetic field, which typically has a rather steep angle with respect to the equatorial plane of the plasma due to the relative strength of the poloidal field compared to that of the toroidal field in spherical tokamaks such as MAST. Note that the intensity of the emission in these filaments is not uniform along their helical axis and that these structures are seen to protrude from the surface as they approach the upper hyperbolic point where they become much more toroidally aligned. These protrusions are consistent with the type of structure predicted by the topology of homoclinic and heteroclinic tangles invoked in the ELM model presented below. Here, the protrusions correspond to the lobes of the tangle, which become narrower in the poloidal direction and more extended in the radial direction as they approach a hyperbolic point (Fig. 5 shows the

lobes calculated when an n=1 homoclinic tangle is found in the DIII-D tokamak). This poloidal compression, accompanied by a radial expansion, is a consequence of the preservation of a constant value of the magnetic flux contained inside each lobe of the structure as prescribed by the Hamiltonian nature of the tangle in the model as it approaches a region of weak poloidal magnetic field near the hyperbolic points. These protruding lobes form a spiraling magnetic footprint that converges to the unperturbed intersection of the separatrix with the divertor target plate similar to the one shown in Fig. 4 of Roeder et al., (2003) for an n=1 homoclinic tangle in DIII-D. These magnetic footprints are essential elements of the nonlinear ELM model presented below.

2.3 ELM theories

Linear ELM theories tend to fall into three general categories. The first and most well developed of these includes ideal and resistive ballooning MHD models. These involve pressure driven modes that couple to external kink modes (sometimes referred to as peeling modes). The second involves dynamics described by a bifurcation of the confinement from an H-mode to an L-mode forming a dynamical state described by a restricted type of limit cycle. The third combines elements taken from the MHD and limit cycle models to construct an appropriate set of dynamics. Each of these models is reviewed in a paper by Conner (1998). Nonlinear ELM models are relatively sparse due to the complex nature of the dynamics and topology involved in this phase of the instability. One example invokes the explosive growth of a narrow finger of hot plasma that pushes its way through other field lines (nonlinear ballooning) from a small region in the plasma interior and spreads across a large section of the surface of the plasma (Cowley et al., 2003). These models are difficult to validate in any practical way with tokamak data due to a lack of specific predictions on how they relate to the various types of ELMs and operating regimes found in high performance tokamak discharges. Clearly, a more quantitative model is needed. Thus, there is strong motivation to develop a model that can be more easily tested with experimental data. The model presented below provides a step in this direction since it can be used to numerically calculate the global topology of ELMs including the distribution and size of magnetic footprints that can be directly compared to divertor diagnostic data (Wingen et al., 2009a).

3. Description of the proposed nonlinear ELM model

3.1 Hamiltonian description of the separatrix topology in poloidally diverted tokamaks

Poloidally diverted tokamaks are formed by a set of external axisymmetric coils that result in poloidal magnetic field nulls when superimposed on the magnetic field due to a toroidal plasma current flow in the discharge. These poloidal field nulls, in combination with magnetic fields from other shaping coils in the tokamak, form hyperbolic points (Zaslavsky, 2005) of the system along with their associated separatrices that divide field line trajectories into trapped (inside the separatrix) versus passing (outside the separatrix) regions of space (Evans, 2008). In an ideal axisymmetric poloidally diverted tokamak the trapped and passing field line regions are referred to as “closed” and “open“ field line regions respectively. This is because field lines outside the separatrix intersect the walls of the tokamak and thus are “open“ with respect to the loss of heat and particles that flow parallel to the field lines. Alternatively, field lines inside the ideal axisymmetric separatrix do not intersect the walls of the tokamak and thus are considered “closed“ in terms of heat and

particle transport parallel to these field lines. As discussed below this terminology is no longer applicable when small non-axsymmetric magnetic pertrubations are present in the system.

A fundamental element of the ELM model discussed here is the nonlinear evolution of the separatrix topology in a poloidally diverted tokamak. Here, the growth of a small topological defect known as a homoclinic tangle (Guckenheimer & Holmes, 1983), formed by the separatrix due to intersections of stable and unstable invariant manifolds associated with a hyperbolic point of the system, is the basic dynamical process invoked by the model. In a poloidally diverted tokamak, following along the spatial trajectory of a stable invariant manifold in the forward direction results in a series of converging steps that approaches the hyperbolic point associated with the manifold. Similarly, following the unstable invariant manifold in the opposite (backward) direction produces a series of converging steps toward the hyperbolic point from the opposite side. Thus, the splitting of trajectories into stable and unstable manifolds due to non-axisymmetric perturbations introduces a directional dependence into the spatial trajectories of the field lines implying that following field lines in opposite directions leads to very different spatial locations in the plasma (with the exception of homoclinic points where the stable and unstable invariant manifolds intersect). In general, a homoclinic (self-intersecting) tangle results in a 3D separatrix topology that is a generic property of perturbed hyperbolic conservative systems which are composed of divergence-free vector fields. The dynamics of such a system is described by integrating Hamilton's equations of motion. Theoretically, it is well known that when sufficiently small perturbations are introduced into such a system it remains Hamiltonian in nature and preserves its well-behaved (deterministic) dynamics (Dankowicz, 1997; Lichtenberg & Lieberman, 1992). Such systems are commonly referred to as "near integrable" and generically have non-degenerate, transversely self-intersecting, separatrix manifold topologies that form the lobes of the homoclinic tangle. Separatrix structures such as these have been studied extensively in physics, mathematics, astrophysics, engineering and neuroscience (Dankowicz, 1997; Guckenheimer & Holmes, 1983; Simiu, 2002). Additionally, it is well known from conservative dynamical systems theory that the topology of a homoclinic tangle is the fundamental element that dictates the behavior of the trajectories which form the solutions to the differential equations describing the dynamics of the system (Guckenheimer & Holmes, 1983). In toroidal plasma confinement devices such as stellarators and tokamaks, the 3D topology of the field lines at any instant in time is found by integrating a set of magnetic differential equations that are formulated in terms of the toroidal (χ) and poloidal (ψ) magnetic flux coordinates (D'haeseler et al., 1991). Here, ψ is associated with the Hamiltonian H while χ serves as the canonical momentum of the system and the equations describing the 3D spatial trajectories of the field lines are given in Hamilton–Jacobi form as:

$$\frac{d\theta}{d\phi} = \frac{dH}{d\chi} \tag{1}$$

$$\frac{d\chi}{d\phi} = -\frac{dH}{d\theta} \tag{2}$$

where θ and ϕ are the poloidal and toroidal angles respectively (Evans, 2008). The usual Hamiltonian is recognized in terms of the familiar canonical coordinates p,q by substituting

$\chi \to p$ and $\theta \to q$ and associating ϕ with time (t). In a tokamak $2\pi\chi$ is the toroidal magnetic flux enclosed by a surface of constant χ and $2\pi\psi = 2\pi H$ is the poloidal magnetic flux inside a surface of constant H.

Equations (1) and (2) are generally integrable given an axisymmetric plasma equilibrium but the addition of small non-axisymmetric magnetic fields transforms the Hamiltonian into an arbitrary function of the toroidal and poloidal angles. In this system a symmetry breaking, non-axisymmetric, magnetic perturbation can be expressed in terms of a perturbed Hamiltonian $\varepsilon H_1(\chi,\phi,\theta)$ where ε is a small dimensionless perturbation parameter. Then, the total Hamiltonian H is given as:

$$H = H_0(\chi) + \varepsilon H_1(\chi,\phi,\theta) \tag{3}$$

or the sum of the axisymmetric part H_0 and the non-axisymmetric perturbed part H_1. The perturbed part of the Hamiltonian can be expressed in terms of a Fourier series as:

$$H_1(\chi,\phi,\theta) = \sum_{m,n} H_{m,n}(\chi)\cos\left(m\theta - n\phi + \chi_{m,n}\right) \tag{4}$$

where m and n are the poloidal and toroidal mode numbers respectively (Abdullaev, 2006).

In realistic tokamaks, the nominally degenerate invariant manifolds that form an ideally axisymmetric separatrix are transformed into an infinite set of homoclinic intersections by small field-errors associated with non-axisymmetric toroidal and poloidal magnetic field coil positions and other random magnetic pertrubations that are an intrinsic part of the tokamak environment (Evans et al., 2005). In addition, externally applied low toroidal mode number (n=1) non-axisymmetric magnetic fields are commonly used to "correct" ambient field-errors that amplify MHD modes in the core plasma.

Figure 5 shows a poloidal projection of the 3D separatrix structure at one toroidal angle in the DIII-D tokamak during the application of an n=1 field-error correction perturbation. As seen in the lower part of Fig. 5(a) just above the divertor region the lobes of the homoclinic tangle intersect the high-field side (HFS) wall (R = 1.02 m, Z = -1.17 m) while on the low-field side (LFS) the lobes intersect the horizontal divertor target plate (R = 1.35 m, Z = -1.36 m). Here, R,Z are cylindrical coordinates representing the distance from the toroidal axis of the tokamak and the displacement from equatorial plane respectively. A magnified view of the lower divertor region is shown in Fig. 5(b) with a 45^o divertor tile (dashed line) connecting the HFS wall (R = 1.02 m) to the horizontal target plate tile (Z = -1.37 m). The entrance to the pump duct is shown on the right-hand side of Fig. 5(b) ($R \geq$ 1.36 m) with the top of the pump duct located at Z = -1.25 m. The connection length L_c of magnetic flux tubes between the LFS divertor target plate and the HFS wall is shown by the color bars in each part of the figure.

This discharge is an example of a double null plasma equilibrium with the balance between the upper and lower hyperbolic points displaced slightly downward. Here, the upper hyperbolic point is located at R = 1.27 m, Z = 1.11 m while the lower hyperbolic point is located at R = 1.28 m, Z = -1.13 m. The topology of the hetroclinic tangles formed in double null equilibria has been shown to be a sensitive function of the relative positions of the upper (secondary) and lower (primary) hyperbolic points (Evans et al., 2004). For a downward biased equilibrium such as that shown in Fig. 5, the homoclinic tangle associated with the lower hyperbolic point dominates the 3D topology of the separatrix and creates a dramatic change in the magnetic topology inside the separatrix. Here, one of the lobes of the

tangle intersects the horizontal divertor target plate at R = 1.36 m, Z = -1.36 m while another lobe intersects the vertical wall located at R = 1.02 m. The intersection of these homoclinic lobes with the divertor target plate and wall "opens" some of the field lines that were previously in the "closed" region inside the separatrix prior to the application of the n=1 magnetic perturbation field from the field-error correction coil (although some field lines are always open due to intrinsic non-axisymmetric field errors without the correction coils). This topological change creates a set of highly complex field line trajectories that traverse the plasma volume inside the separatrix and connect the vertical high-field side (HFS) wall to the low-field side (LFS) horizontal divertor target plate. This topology is similar to that of "line-tying" found in the solar photosphere (Gibons & Spicer, 1981). Additionally, the field line topology formed by this "line-tying" type of bifurcation is composed of a mixture of stochastic fields, with a wide range of connection lengths (L_c) that form fractal distributions (Abdullaev, 2006), embedded inside a set of coherent flux tubes with short connection lengths (Wingen et al., 2009b; Wingen et al., 2009c). It is the short L_c flux tubes that play a fundamental role in the nonlinear ELM model discussed below.

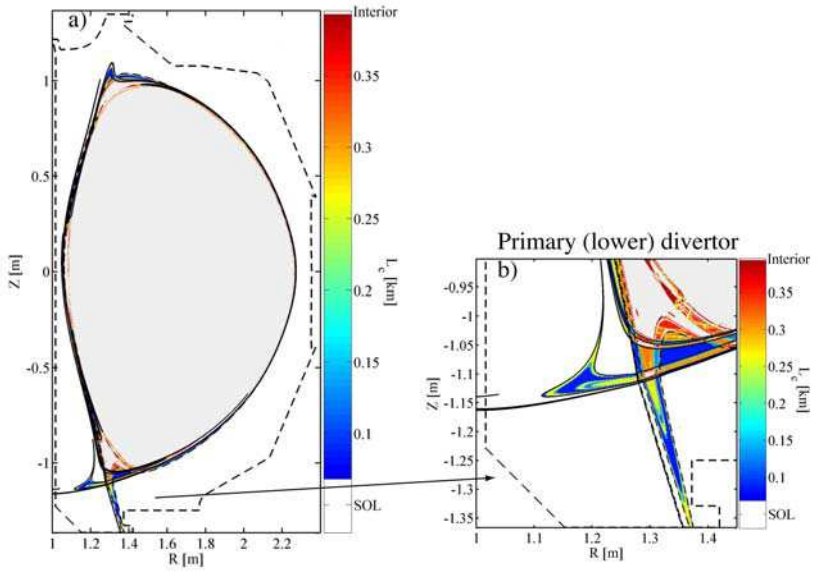

Fig. 5. (a) Full poloidal cross sectional view of a separatrix homoclinic tangle formed by an applied external n=1 magnetic perturbation due to the DIII-D field-error correction coil with a current of 8 kAt in discharge 133908 at t = 2000 ms. (b) An expanded cross sectional view of the primary divertor. L_c is the field line connection length between the horizontal target plate (Z = -1.36 m) and the vertical wall (R = 1.02 m).

The intersection of the homoclinic and heteroclinic lobes with divertor targets and walls forms objects referred to as magnetic footprints on the R,ϕ and Z,ϕ planes of the divertor targets and walls respectively as shown in Fig. 6(a) for the HFS wall and Fig. 6(b) for the LFS divertor target plate for the same conditions as in Fig. 5. Measurements of the heat (Evans et al., 2005, Evans et al., 2007) and particle (Schmitz et al., 2008) flux distributions on the

DIII-D divertors have been shown to be qualitatively consistent with numerical calculations of magnetic footprints produced by homoclinic lobes during experiments with applied non-axisymmetric magnetic fields from field-error correction and edge MHD (ELM) suppression coils (Evans et al., 2006). Similar heat flux patterns have been observed in the ASDEX-U tokamak (Eich et al., 2005) during ELMs. Quantitative comparisons of heat flux measurements inside these footprints with numerical simulations indicate that the separation between adjacent lobe intersections with the divertor targets can be a factor of 2-3 times larger than that predicted suggesting that there is a significant amplification of the homoclinic tangle structure from the applied n=1 field due to the response of the plasma (Evans et al., 2007). There are also indications that the topology of the lobes is affected by magnetic perturbations from MHD modes deep in the core plasma (Evans et al., 2005).

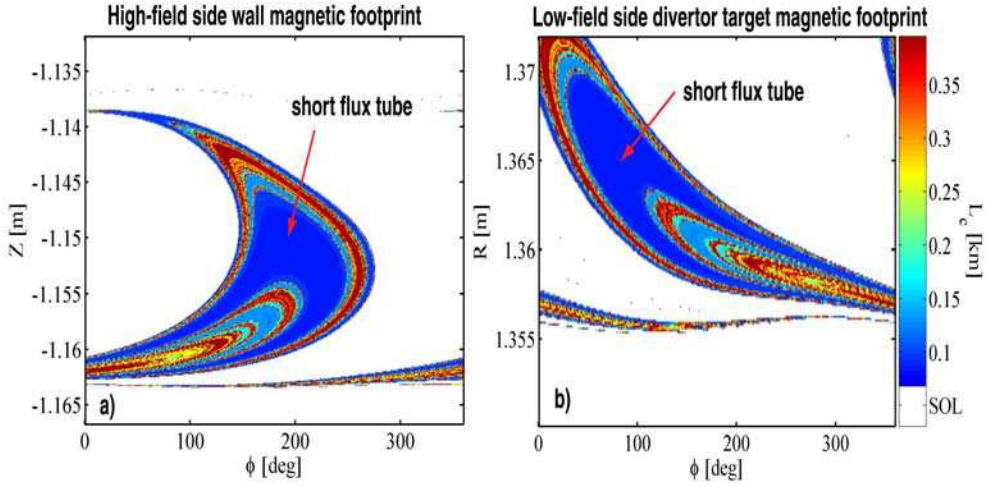

Fig. 6. Lower divertor (a) magnetic footprint formed on HFS vertical wall by an externally applied n=1 perturbation (no plasma response) from the DIII-D field-error correction coil with a current of 8 kAt in discharge 133908 at t = 2000 ms and (b) the LFS magnetic footprint formed on the horizontal divertor target plate. These footprints define the open field line hit points due to the intersection of the lobes of the homoclinic tangle shown in Fig. 5 with the target plate and wall. As in Fig. 5, L_c is the field line connection length between the horizontal target plate (Z = -1.36 m) and the vertical wall (R = 1.02 m).

3.2 Description of the temporal evolution prescribed by the model

A conceptual model describing the dynamics of the edge plasma and the evolution of the pedestal magnetic topology following the linear growth phase of a type-I ELM is presented. Understanding the physics, topology and dynamics of ELMs during their post-linear growth phase is essential for predicting the characteristics of these instabilities as a funtion of the pedestal plasma conditions. In particular, a model is needed that can be used to predict the temporal evolution of the plasma heat and particle distributions on the vessel wall and divertor components.

As discussed above, small quasi-static homoclinic and heteroclinic tangles result naturally from a variety of non-axisymmetric magnetic field perturbations commonly found in high

performance poloidally diverted tokamaks. Examples of these non-axisymmetric field perturbations include toroidal field ripple, field-errors, core and edge MHD modes, 3D electromagnetic field control (trim) coils and small, spatially random, 3D field components due to magnetic materials and tolerence build-ups in the electromagnetic coils used to confine and shape the plasma (Evans et al., 2005; Evans et al., 2007). Thus, it is not unreasonable to expect the formation of separatrix homoclinic and heteroclinic tangles to be the norm rather than the exception, whether in a low confinement L-mode or in high confinement H-mode plasma as well as between and during ELMs. It is the existence of the separatrix topology associated with these tangles between ELMs that forms the basis of the model (Evans et al., 2009) described here.

Given the basic topology shown in Fig. 5, the model assumes that small fluctuations in the pedestal plasma pressure initiate a linearly growing MHD instability as the equilibrium conditions in a narrow region just inside the separatrix approach a marginal stability point. An example of this process is described by ideal MHD peeling-ballooning theory (Snyder et al., 2005; Wilson et al., 2006) which presumes that linearly growing intermediate n modes lead to the onset of the nonlinear growth phase. Peeling-ballooning theory predicts that the onset of this edge MHD mode significantly increases the radial heat and particle transport. Our model assumes that the energy associated with the linearly growing MHD mode flows into the coherent, short connection length, homoclinic flux tubes connecting the HFS wall and the LFS divertor target. At this point, fast parallel transport along these homoclinic flux tubes causes a rapid increase in the electron temperature (T_e) inside the magnetic footprints near the wall and divertor surfaces. Experimental measurements taken during the early growth of an ELM demonstrate that there is a rapid release of thermal energy from the area located near the steep gradient region leading up to the top of the pedestal just inside the separatrix (Kirk et al., 2007, Neuhauser et al., 2008). These observations are consistent with our requirement of a rapid increase in the radial energy transport during this time. These rapid bursts of energy flowing from the pedestal into the divertor appear to be correlated with an increase in broadband magnetic fluctuations in the pedestal starting about 10 μs before the onset of the nonlinear growth phase (Neuhauser et al., 2008) suggesting that currents in this region may play a key role in the onset of the nonlinear growth phase.

In our model, it is these inital heat pulses associated with the linearly growing MHD instability that provide the mechanism needed to form a feedback amplification loop. It is this feedback loop that causes the stable and unstable invariant manifolds of the initial homoclinic tangle to grow explosively. Here, it is presumed that the amplification process is triggered by the formation of field-aligned thermoelectric currents that flow through the short, pedestal plasma, homoclinic flux tubes connecting the inner wall and outer divertor target plate. These thermoelectric currents form when T_e at one end of a flux tube increases relative to T_e at the other end (Staebler & Hinton, 1989). Since part of the heat pulse enters the short flux tube near the equatorial plane on the LFS of the discharge it is expected to arrive at the LFS target well before arriving at the HFS wall. Numerical simulations of these two-poloidal-turn helical flux tubes (Wingen, et al. 2009a) show that the distance from the LFS equatorial plane to the LFS target plate is ~25 m while the distance to the HFS wall is ~75 m. In DIII-D H-mode plasmas, T_e just inside the separatrix, where these flux tubes reside, is ~400-500 eV. Thus, given an electron thermal velocity $v_{\mathrm{Te}} = (kT_e/m_e)^{1/2} = 8.4\times10^6$ m/s where k is Boltzmann's constant and m_e is the mass of an electron, these heat pulses arrive at the LFS target plate approximately 6 μs before reaching the HFS wall. This

causes T_e near the LFS target plate to increase relative to that near the HFS wall and initiates the flow of a thermoelectric current from the LFS target to the HFS wall with a return current connecting through the lower divertor vessel structure.

Thus, the model assumes that following the release of the initial heat pulse from the linearly growing MHD mode a small field-aligned thermoelectric current begins to flow in a helical flux tube formed by a small preexisting homoclinic tangle. Although the time evolution of the current growth is not specifically predicted by the model, it is assumed that as the current grows its magnetic field perturbs the upper and lower hyperbolic points causing the lobes of the homoclinic tangle and their associated magnetic footprints to increase in size. Simulations have been carried out assuming the current density in the flux tube is limited to approximately 1/2 the initial ion saturation current density (~70-80 mA/mm^2) during the nonlinear phase of the instability (Wingen, et al., 2009a). These simulations have shown that the magnetic footprint, associated with a single n=1 flux tube connecting the primary (lower) LFS divertor target with the HFS wall, grows from an area of 1760 mm^2, with a current of 135.5 A, to an area of 3564 mm^2 with a current of 274.4 A. During this process, a topological bifurcation takes place that creates a new set of n=2 flux tubes connecting the primary divertor LFS target to the HFS wall (Wingen, et al., 2009a). It is then assumed, that as the thermoelectric current grows with increasing footprint area there is a commensurately increasing flow of energy from the pedestal into the flux tube that maintains the constant current density. Here, the working hypothesis is that the growing helical thermoelectric current filaments associated with the short connection length flux tubes also produce resonant magnetic field components that open magnetic islands (*i.e.*, Poincaré islands) on rational surfaces across the pedestal region in addtion to perturbing the nominally axisymmetric hyperbolic points. As these islands grow and overlap they produce an increase in the local magnetic field line stochasticity which enhances the effective radial heat tranport into the homoclinic flux tube containing the thermoelectric current. This completes the feedback amplification loop and results in the initial explosive growth phase of the topological instability.

During the next step in the process, the initial helical current filament grows explosively and acts to amplify the lobes of the homoclinic tangle while inducing a growing level of pedestal stochasticity that penetrates deeper into the core plasma as it grows. This process results in a self-amplification of the lobes due to a positive feedback loop between the size of the tangle lobes, an increasing stochastic layer width and an increase in the heat flux to the target plates that drives an increasing flow of current. This process takes on the appearance of growing helical filaments that protrude beyond the edge of the plasma and seem to propagate radially outward as they grow. A key feature of the processes involved up to this point is that there is no need to invoke field line tearing and reconnection during the evolution of an ELM. The entire process can be described using ideal MHD theory without requiring resistive or dissipative effects that would cause the filaments to tear and separate from the edge of the plasma. Such a process would rapidly shut down the thermal transport responsible for the growth of the instability. This is seen by comparing the 1-2 ms decay time following the current peak in Fig. 3 to a tearing mode growth time $\gamma^{-1} \sim \tau_r^{3/5}\tau_A^{2/5}$ s where γ is the growth rate of the tearing mode, τ_r is the resistive time and τ_A is the Alfvén time in the pedestal. We find that $\gamma^{-1} \leq 0.1$ ms where $\tau_r = 1.2\text{x}10^{-4}$ s and $\tau_A = 5.8\text{x}10^{-5}$ s or approximately an order of magnitude shorter than the current decay time. Therefore, the

growth of a tearing mode following the peak in the current would cause a separation of the filament from the pedestal and a rapid, sub-millisecond, termination of the of the current. Instead, we see that the ELM is a radially extended structure, as indicated by the relatively constant ratio of the signals from two adjacent Langmuir probes in Fig. 3, which is reminiscent of the lobes of a homoclinic tangle and that this radial structure persists as the current slowly decays. This relatively slow decay of the current is more consistent with a slow shutdown of the heat flux from the pedestal as the energy reservoir in this region is slowly depleted and T_e in the short flux tubes drops. This reduction in T_e causes an increase in resistivity in the short flux tubes which, when coupled with a cooling of the plasma in front of the divertor target plate due to an increase in particle recycling, as shown in Fig. 2, slowly reduces the thermoelectric current flowing between the target plate and the wall.

Numerical simulations of the growth experienced by a pre-existing, field-error related, homoclinic tangle have been carried out using current filaments that are proportional to the area of the magnetic footprint on the divertor target plate. Results from these simulations demonstrate that the calculated nonlinear dynamics of the tangle's topology are consistent with the heat flux patterns measured in the DIII-D divertor during a type-I ELM (Wingen et al., 2009a). A key question studied during these simulations addresses how the topological evolution prescribed by the model conforms to experimental measurements of type-I ELM dynamics. In particular, data such as that shown in Fig. 4 suggest that the peak in the toroidal mode spectrum of an ELM increases in mode number during the nonlinear growth phase. As discussed below, a bifurcation in the separatrix topology has been identified during the early growth phase of the instability. This bifurcation involves the appearance of heteroclinic invariant manifolds associated with the upper (secondary) hyberbolic point.

3.3 Dynamics of an ELM-induced homoclinic-to-heteroclinic separatrix bifurcation

Here, we describe the appearance of a homoclinic-to-heteroclinic bifurcation as the total current flowing in a short flux tube, connecting the LFS divertor target plate to the HFS wall, increases from 100 to 300 A. The simulation starts with an axisymmetric plasma equilibrium. We then superimpose a spectrum of nonaxisymmetric magnetic perturbations due to field-errors that have been systematically measured in the DIII-D tokamak (Luxon et al., 2003) along with a 3D magnetic perturbation field produced by a field-error correction coil (referred to as the I-coil) in DIII-D discharge 133908 at t = 2000 ms (Wingen et al., 2009a). Note that this is the same plasma equilibrium shown in Fig. 5 but there an artificial n=1 nonaxisymmetric magnetic field is applied by a coil referred to as the C-coil with a relatively large current in order to highlight the properties of the homoclinic tangle. In the simulation discussed here, we use the actual coil currents that were employed during the experiment in discharge 133908.

As a starting point for this simulation, the shortest flux tube produced by the field-errors and an n=1 correction coil is selected. Initially, there is only one relatively small flux tube connecting the LFS side lower (primary) divertor target plate with the HFS wall. We refer to this as flux tube number 1. This flux tube makes two poloidal revolutions along its path through the pedestal plasma just inside the separatrix and has a total length from the target plate to the wall of ~100 m. The current flowing in a large divertor tile sensor is used to establish a current density calibration for the simulation. This is done by calculating the area

of overlap between the tile sensor and the magnetic footprint at the toroidal and radial position of the tile when the maximum current during an ELM is reached. Using the calculated area of intersection with the tile sensor and an assumed current density of 77 mA/mm^2 we get 200 A which agrees with the measured current in this tile sensor at the peak amplitude of the ELM. The assumed current density (about 1/2 the pre-ELM ion saturation current) is held fixed throughout the remainder of simulation while the topology of the separatrix unfolds. We start with a relatively small current in flux tube number 1 and increase the current in steps. With each iteration of the code, the area of the magnetic footprints increases as the size of the lobes produced by the homoclinic tangle associated with the primary divertor hyperbolic point increases. The current is increased until the total area of all the magnetic footprints overlapping the tile sensor equals ~3000 mm^2. At this point, the area of the three footprints associated with flux tubes 1, 2 and 3 is calculated and using the assumed current density of 77 mA/mm^2 a total current of ~4.9 kA is obtained (Wingen et al., 2009a).

During the sequence of iterations in the current flowing in flux tube number 1, a new pair of flux tubes is formed followed by the formation of a fourth flux tube at a higher current. The first pair of flux tubes, referred to as flux tube number 2 and 3, connect the primary LFS divertor target plate to the HFS wall after one poloidal turn and have a length of ~50 m. Flux tubes 2 and 3 are formed during a bifurcation of the separatrix topology that involves a splitting of the invariant manifolds, caused by the presence of the secondary (upper) hyperbolic point, into a higher order set of stable and unstable branches of the original manifold topology. We refer to this as a homoclinic-to-heteroclinic bifurcation although here we focus only on the increased complexity of the homoclinic tangle associated with the primary (lower) hyperbolic point.

Figure 7(b) shows the structure of the manifolds produced by the primary (lower divertor) hyperbolic point in the secondary divertor region near the upper hyperbolic point with a current of 100 A flowing in flux tube number 1. Flux tube number 1 is not large enough to be clearly identified at this level of current. With this current, the initial formation of flux tubes 2 and 3 has begun. Here, flux tubes are formed in the area between intersecting stable and unstable manifolds. As seen in Fig. 8(a) flux tube number 3 is completed at 130 A when the stable and unstable manifolds intersect while flux tube number 2 is not yet fully formed at 150 A in Fig. 8(b).

As the current in flux tube number 1 is increased from 150 A to 200 A, flux tube number 2 is completed and a new partially formed flux tube appears, flux tube number 4 as shown in Fig. 9(a), on each side of flux tube number 2. Between 200 A and 300 A flux tube number 4 is completed and manifold connections are made between the secondary (upper) divertor LFS target plate and the primary (lower) HFS wall as well as between the primary LFS target plate and the secondary HFS wall as shown in Fig. 9(b).

From this point on in the simulation a current proportional to the area of intersection of flux tubes 2 and 3 with the primary LFS divertor target, having a current density of 77 mA/mm^2, is included at each subsequent step until the current limit discussed above is reached. As the simulation proceeds flux tubes 2 and 3, which form a pair of single poloidal turn helical structures that are displaced from each other toroidally by 180^o, produce an n=2 perturbation that dominates the growth of the lobes and the primary divertor LFS target plate magnetic footprints.

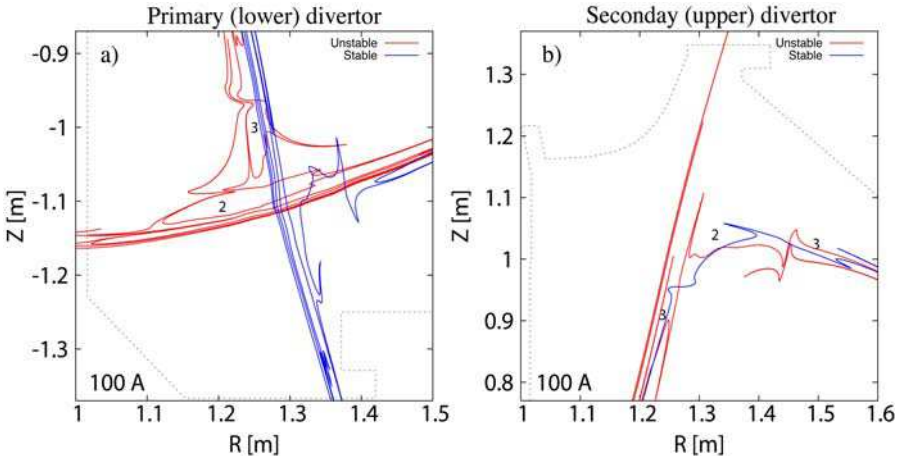

Fig. 7. Poincaré plots of (a) the calculated structure of the stable and unstable invariant manifolds in the primary divertor with a current of 100 A in flux tube number 1 (not clearly visible) and (b) the corresponding structure of the manifolds in the secondary divertor. The numbers 2 and 3 indicate regions where flux tube number 2 and 3 will form as the current in flux tube number 1 is increased in the simulation once the stable and unstable manifolds intersect.

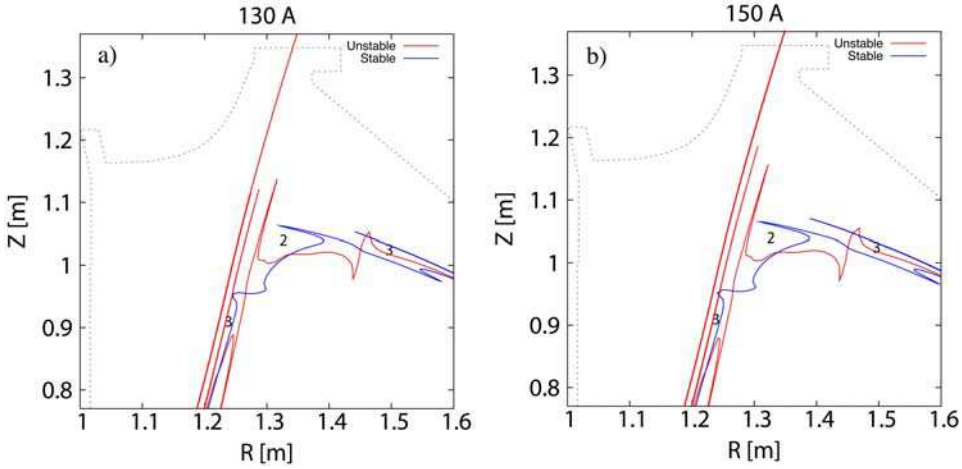

Fig. 8. Poincaré plots of (a) the formation of flux tube number 3 in the secondary divertor as the current in flux tube 1 is increased to 130 A, (b) flux tube number 2 is not completely formed at 150 A.

4. Discussion and conclusion

A conceptual model describing the nonlinear gowth of type-I ELMs in high performance tokamak plasmas has been presented along with a numerical simulation of the separatrix evolution, described by the model, during an ELM in a typical DIII-D H-mode plasma. The

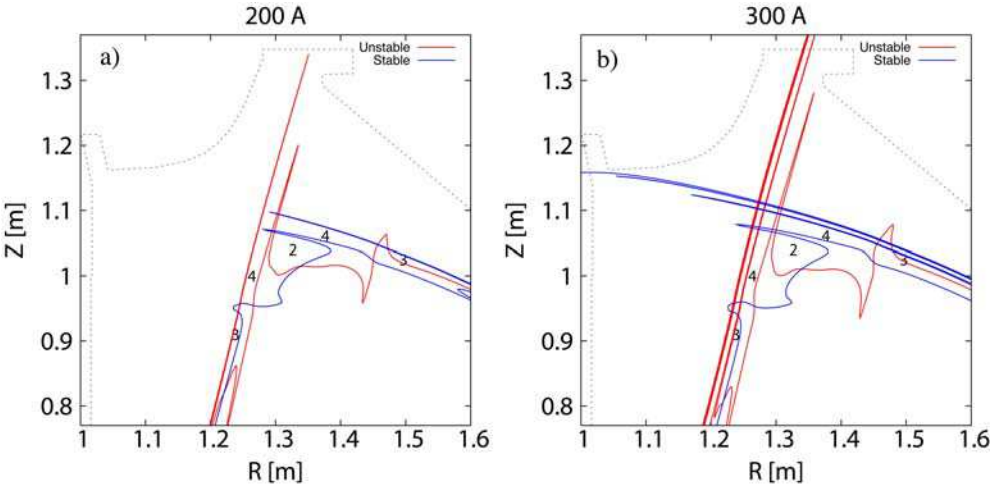

Fig. 9. Poincaré plots of (a) the formation of flux tube number 2 in the secondary divertor at 200 A in flux tube number 1 and the appearance of a new partially formed flux tube (number 4) while (b) at 300 A in flux tube number 1 all of the new flux tubes (numbers 2, 3 and 4) are fully formed.

temporal evolution of the separatrix is driven by a plasma instability resulting from a rapidly growing current that flows through the pedestal region of the plasma and changes the global topology of the manifolds that make up the separatrix. This topological change involves a homoclinic-to-heteroclinic bifurcation of the secondary (upper) hyperbolic point in the equilibrium magnetic field. The bifurcation creates an n=2 helical structure, consisting of two independent flux tubes separated by 180º toroidally, early in nonlinear growth phase when a small, 150-200 A, field-aligned current flows in the original n=1 flux tube created by field-errors and a field-error correction coil. Although reversing the direction of the current in the n=1 flux tube does not have a significant effect on the structure of the invariant manifolds associated with the tangle structures, distributing the current into multiple filaments rather than allowing it in the single filament, as in the simulation shown in Sec. 3.3, results in a much more complex topology that has significantly more lobes intersecting the primary LFS divertor target plate. Thus, the model predicts the formation of a new set of invariant manifolds associated with the secondary hyperbolic point. These new invariant manifolds intersect the upper (secondary) divertor target plate and the HFS wall in DIII-D during the nonlinear growth phase of an ELM. This has significant implications for fusion reactor designs since it implies that complex heat and particle flux striations, associated with the magnetic footprints and flux tubes due to these new separatrix manifolds, should cause large impulsive energy bursts on secondary plasma facing surfaces that are not typically designed to handle such interactions with high energy density plasmas. Therfore, it is important that these predictions be tested using high time resolution measurements of the transient heat and particle flux interactions with plasma facing components near the secondary hyperbolic point during ELMs.

Another important question to ask of the model is whether it can be used to shed light on the physics of ELM suppression when small (~50 G), stationary, n=3 magnetic pertrubations are applied to ELMing H-modes in the DIII-D tokamak (Evans et al, 2006). Here, an interesting

hypothessis that can be tested is that the n=3 field interacts with the lobes of the n=1 field-error tangle causing them to break up into relatively small scale structures that are more effective for dissapating the steady-state heat and particle flux over a much larger area of the divertor. This is expected to provide additional control over the pedestal transport that could be used to keep the pressure gradient below the threshold required for the onset of the linearly growing MHD installability. Constructive and destructive interference between nonaxisymmetric magnetic pertrubations from various coils in DIII-D has been studied previously. This work demonstrated that such interactions lead to much more complex lobe structures (Wingen et al., 2009b) that tends to spread the footprints and open more flux tubes (Evans et al, 2007) which can be used to fine tune the pedestal transport. Extending this hypothesis to higher n homoclinic structures, such as n=4 up to n=6 or 7 or combinations of structures with toroidal mode numbers ranging from 1 thorugh 7, suggests that the effect may provide much better control over the height and width of the pedestal region thus allowing the possibility of fine tuning of the pressure gradient profile. With advanced realtime pedestal profile diagnostics, it should be possible to combine this multimode perturbation field approach with an edge pressure and current gradient tracking algorithm to obtain a desired set of pedestal properties, particularly if an edge-localized heating and current drive system such as electron cyclotron system, were to be included as part of the feedback loop.

In general, the model presented here qualitatively fits some of the observed experimental attributes of large type-I ELMs such as a slow decay rate of the current in the flux tube as seen in Fig. 3. The model also has elements that may explain the variability seen in ELM signatures such as the divertor recycling emissions when effects such as type-II ELMs between the type-I ELMs are included. Other effects, such as an increase in the frequency of the ELMs with increasing heating power and the apprent rotation of the ELM structure during the nonlinear growth phase, have not yet been addressed by the model. These will be the focus of future work along with more detailed experimental comparisons.

5. Acknowledgments

This work was supported by the US Department of Energy under DE-FC02-04ER54698, DE-AC04-94AL85000, and DE-AC52-07NA27344.

6. References

Abdullaev, S.S. (2006). *Construction of Mappings for Hamiltonian Systems and Their Applications,* Lecture Notes in Physics, Vol. 691, Springer, ISBN-10 3-540-30915-2, Berlin.

Boedo, J.A.; Rudakov, D.L.; Hollmann, E.M.; Gray, D.S.; Burrell, K.H.; *et al.* (2005). Edge-localized mode dynamics and transport in the scrape-off layer of the DIII-D tokamak. *Physics of Plasmas* 12, 072516:1-11.

Callen, J.D.; Carreras, B.A.; & Stambaugh, R.D. (1992) Stability and transport processes in tokamak plasmas. *Physics Today* 45, 34-42.

Connor, J.W. (1998). A review of models for ELMs. *Plasma Physics and Controlled Fusion* 40, 191-213.

Cowley, S.C.; Wilson, H.; Hurricane, O & Fong, B. (2003). Explosive instabilities: from solar flares to edge localized modes in tokamaks. *Plasma Physics and Controlled Fusion* 45, A31-A38.

Dankowicz, H. (1997). *Chaotic Dynamics in Hamiltonian Systems with applications to celestial mechanics*, World Scientific Series on Nonlinear Science, Series A, Vol. 25, World Scientific, ISBN 9810232217, Singapore.

D'haeseleer, W.D.; Hitchon, W.N.G.; Callen, J.D. & Shohet, J.L. (1991). *Flux coordinates and magnetic field structure, a guide to a fundamental tool for plasma theroy*, Springer Series in Computational Physics, Springer-Verlag ISBN 3-540-52419-3, Berlin.

Eich, T.; Herrmann, A.; Neuhauser, J.; Dux, R.; Fuchs, J.C.; *et al.* (2005). Type-I ELM structure on divertor target plates in ASDEX Upgrade. *Plasma Physics and Controlled Fusion* 47, 815-842.

Evans, T.E.; Lasnier, C.J.; Hill, D.N.; Leonard, A.W.; Fenstermacher, M.E.; et al. (1995). Measurements of non-axisymmetric effects in the DIII-D divertor. *Journal of Nuclear Materials* 220-222, 235-239.

Evans, T.E.; Moyer, R.A.; Stephan, E.A.; Snider, R.T. & Coles, W.A. (1996). Causal spacio-temporal correlations of short scale length solar wind accelaration and heating mechanisma with a solar event correlation analyzer (SECA) instrument package. *Robotic exploration close to the sun: scientific basis*, AIP Conference Proceedings 385, pp. 145-152, Editor: S. R. Habbal, American Institute of Physics ISBN 1-56396-618-2, New York.

Evans, T.E.; Roeder, R.K.W.; Carter, J.A. & Rapoport, B.I. (2004). Homoclinic tangles, bifurcations and stochasticity in poloidally diverted tokamaks. *Contributions to Plasma Physics* 44, 235-240.

Evans, T.E.; Roeder, R.K.W.; Carter, J.A.; Rapoport, B.I.; Fenstermacher, M.E.; & Lasnier, C.J. (2005). Experimental signatures of homoclinic tangles in poloidally diverted tokamaks. *Journal of Physics: Confonference Proceedings Series* 7, 174-190.

Evans, T.E.; Moyer, R.A.; Burrell, K.H.; Fenstermacher, M.E.; Joseph, I.; et al. (2006). Edge stability and transport control with resonant magnetic pertrubations in collisionless tokamak plasmas. *Nature Physics* 2, 419-423.

Evans, T.E.; Joseph, I.; Moyer, R.A.; Fenstermacher, M.E.; Lasnier, C.J.; Yan, L.W. (2007). Experimental and numerical studies of seperatrix splitting and magnetic footfrints in DIII-D. *Journal of Nuclear Materials* 363-365, 570-574.

Evans, T.E. (2008). Implications of topological complexity and Hamiltonian chaos in the edge magnetic field of toroidal fusion plasmas. *Chaos, Complexity and Transport: Theory and Applications*, pp. 147-176 Edited by: Chandre C.; Leoncini, X. & Zaslavsky, G. World Scientific Press, ISBN-13 978-981-281-897-9, Singapore.

Evans, T.E.; Yu, J.H.; Jakubowski, M.W.; Schmitz, O.; Watkins, J.G. & Moyer, R.A. (2009). A coneptual model of the magnetic topology and nonlinear dynamics of ELMs. *Journal of Nuclear Materials* 390-391, 789-792.

Fenstermacher, M.E.; Leonard, A.W.; Snyder, P.B.; Boedo, J.A.; Brooks, N.H.; et al., (2003). ELM particle and energy transport in the SOL and divertor of DIII-D. *Plasma Physics and Controlled Fusion* 45, 1597-1626.

Gibons, M. & Spicer, D.S. (1981). On line tying. *Solar Physics* 69, 57-61.

Guckenheimer, J. & Holmes, P. (1983). *Nonlinear Oscillations, Dynamical Systems, and Bifurcations of Vector Fields,* Applied Mathematical Science, Vol. 42 Springer-Verlag, ISBN 0-387-90819-6, New York.

Kirk, A.; Wilson, H.R.; Counsell, G.F.; Akers, R.; Arends, E.; et al. (2004). Spatial and temporal structure of edge-localized modes. *Physical Review Letters* 92, 245002:1-4.

Kirk, A.; Counsell, G.F.; Cunningham, G.; Dowling, J.; Dunstan, M.; et al. (2007). Evolution of the pedestal on MAST and the implications fo ELM power loadings. *Plasma Physics and Controlled Fusion* 49, 1259-1275.

Lichtenberg, A.J. & Lieberman, M.A. (1992). *Regular and Chaotic Dynamics*, Applied Mathematical Sciences, Vol. 38 second edition Springer-Verlag, ISBN 0-387-97745-7, New York.

Loarte, A.; Saibene, G.; Sartori, R.; Becoulét, M.; Horton, L.; et al. (2003). ELM energy and particle losses and their extrapolation to burning plasma experiments. *Journal of Nuclear Materials* 313-316, 962-966.

Luxon, J.L. (2002). A design retrospective of the DIII-D tokamak. *Nuclear Fusion* 42, 614-633.

Luxon, J.L.; Schaffer, M.J.; Jackson, G.L.; Leuer, J.A.; Nagy, A.; et al. (2003). Anomalies in the applied magnetic fields in DIII-D and their implications for the understanding of stability experiments. *Nuclear Fusion* 43, 1813-1828.

Maingi, R.; Bush, C.E.; Fredrickson, E.D.; Gates, D.A.; Kaye, S.M.; (2005). H-mode pedestal, ELM and power threshold studies in NSTX. *Nuclear Fusion* 45, 1066-1077.

Neuhauser, J.; Bobkov, V.; Conway, G.D.; et al. (2008). Structure and dynamics of spontaneous and induced ELMs on ASDEX Upgrade. *Nuclear Fusion* 48, 045005:1-15.

Osborne, T. H.; Ferron, J.R.; Groebner, R.J.; Lao, L.L.; Leonard, A.W.; et al. (2000). The effect of plasma shape on H-mode pedestal characteristics on DIII-D. *Plasma Physics and Controlled Fusion* 42, A175-A184.

Roeder, R.K.W.; Rapoport, B.I. & Evans, T.E.; (2003). Elplicit calcualtions of homoclinic tangles in tokamaks. *Physics of Plasmas* 10, 3796-3799.

Simiu, E. (2002). *Chaotic Transitions in Deterministic and Stochastic Dynamical Systems*, Princeton Series in Applied Mathematics, Princeton University Press, ISBN 0-691-05094-5, Princeton, New Jersey.

Schmitz, O.; Evans, T.E.; Fenstermacher, M.E.; Frerichs, H.; Jakubowski, M.W.; et al. (2008). Aspects of three dimensional transport for ELM control experiments in ITER-similar shape plasmas at low collisionality in DIII-D. *Plasma Physics and Controlled Fusion* 50, 124029:1-19.

Snyder, P.B.; Wilson, H.R. & Xu, X.Q. (2005). Progress in the peeling-ballooning model of edge localized modes: Numerical studies of the nonlinear dynamics. *Physics of Plasmas* 12, 056115:1-7.

Staebler , G.M. & Hinton, F.L. (1989). Currents in the scrape-off layer of diverted tokamaks. *Nuclear Fusion* 29, 1820-1824.

Suttrop, W. (2000). The physics of large and small edge localized modes. *Plasma Physics and Controlled Fusion* 42 pp. A1-A14.

Wesson, J. (2004). *Tokamaks*, 3rd Ed. Oxford University Press, ISBN 0-19-8509227, New York.

Wilson, H.R.; Cowley, S.C.; Kirk, A.; & Snyder, P.B. (2006). Magnetohydrodynamic stability of the H-mode transport barrier as a model for edge localized modes: an overview. *Plasma Physics and Controlled Fusion* 48, A71-A84.

Wingen, A.; Evans, T.E.; Lasnier, C.J. & Spatschek, K.H. (2009a). Numerical modelling of the nonlinear ELM cycle in tokamaks. *Physical Review Letters* Vol. -- pp. – (submitted).

Wingen, A.; Evans, T.E. & Spatschek, K.H. (2009b). High resolution numerical studies of the separatrix splitting due to non-axisymmetric perturbation in DIII-D. *Nuclear Fusion* 49, 055027:1-8.

Wingen, A.; Evans, T.E. & Spatschek, K.H. (2009c). Footprint structures due to resonant magnetic perturbations in DIII-D. *Physics of Plasmas* 16, 042504:1-5.

Yu, J.H.; Boedo, J.A.; Hollmann, E.M.; Moyer, R.A. & Rudakov, D.L. (2008). Fast imaging of edge localized mode structure and dynamics in DIII-D. *Physics of Plasmas* 15, 032504:1-7.

Zaslavsky, G.M. (2005). *Hamiltonian chaos & fractional dynamics*, Oxford University Press ISBN 0-19-852604-0, Oxford.

Zohm, H. (1996). Edge localized modes (ELMs). *Plasma Physics and Controlled Fusion* 38, 105-128.

Nonlinear Dynamics

Edited by Todd Evans

ISBN 978-953-7619-61-9
Hard cover, 366 pages
Publisher InTech
Published online 01, January, 2010
Published in print edition January, 2010

This volume covers a diverse collection of topics dealing with some of the fundamental concepts and applications embodied in the study of nonlinear dynamics. Each of the 15 chapters contained in this compendium generally fit into one of five topical areas: physics applications, nonlinear oscillators, electrical and mechanical systems, biological and behavioral applications or random processes. The authors of these chapters have contributed a stimulating cross section of new results, which provide a fertile spectrum of ideas that will inspire both seasoned researches and students.

InTech Europe
University Campus STeP Ri
Slavka Krautzeka 83/A
51000 Rijeka, Croatia
Phone: +385 (51) 770 447
Fax: +385 (51) 686 166
www.intechopen.com

InTech China
Unit 405, Office Block, Hotel Equatorial Shanghai
No.65, Yan An Road (West), Shanghai, 200040, China
中国上海市延安西路65号上海国际贵都大饭店办公楼405单元
Phone: +86-21-62489820
Fax: +86-21-62489821